



1 **Observational evidence of particle condensational**
2 **growth in the UTLS over Tibetan Plateau**

3

4 **Qianshan He^{1,2}, Jianzhong Ma³, Xiangdong Zheng³, Xiaolu Yan³, Holger**
5 **Vömel⁴, Frank G. Wienhold⁵, Wei Gao^{1,2}, Dongwei Liu^{1,2}, Guangming Shi⁶,**
6 **Tiantao Cheng⁷**

7 ¹Shanghai Meteorological Service, Shanghai, China

8 ²Shanghai Key Laboratory of Meteorology and Health, Shanghai, China

9 ³State Key Laboratory of Severe Weather & CMA Key Laboratory of Atmospheric
10 Chemistry, Chinese Academy of Meteorological Sciences, Beijing, China

11 ⁴Earth Observing Laboratory, National Center for Atmospheric Research, Boulder, CO,
12 USA

13 ⁵ETH Zurich, Institute for Atmospheric and Climate Science (IAC), CH-8092 Zurich,
14 Switzerland.

15 ⁶Chongqing Institute of Green and Intelligent Technology, Chinese Academy of
16 Sciences, Chongqing, China

17 ⁷Department of Atmospheric and Oceanic Sciences, Institute of Atmospheric Sciences,
18 Fudan University, Shanghai, China

19 Correspondence to: Jianzhong Ma (majz@cma.gov.cn)

20

21 **Key Points:**

22 1. Balloon-borne measurements show an enhanced aerosol layer consisting dominantly
23 of fine particles in the UTLS over Tibetan Plateau.

24 2. Water vapor plays an important role in the growth of these fine particles.

25

26 **Abstract**

27 We measured the vertical profiles of aerosol backscattering ratio (BSR) with a
28 balloon-borne lightweight COBALD at Linzhi, located in the southeastern Tibetan
29 Plateau, in the summer of 2014. An enhanced aerosol layer in the upper
30 troposphere/lower stratosphere (UTLS), with BSR (455 nm)>1.1 and BSR (940
31 nm)>1.4, was observed. The Color Index (CI) of the enhanced aerosol layer, defined as
32 the ratio of aerosol backscatter ratios at wavelengths of 940 nm and 455 nm, varied



1 from 4 to 8, indicating the prevalence of dominant fine particles with mode radius less
2 than 0.1 μm . We find that except for the very small particles (mode radius smaller than
3 0.04 μm) at low relative humidity ($\text{RH}_i < 40\%$), the relatively large particles in the
4 aerosol layer were generally very hydrophilic as their size increased dramatically with
5 relative humidity. This result indicates that water vapor can play a very important role
6 in the formation of large amounts of fine particles in the UTLS over the Tibetan Plateau.
7 Our observations provide observation-based evidence supporting that the aerosol
8 particle condensational growth is an important process for the summer ATAL
9 enhancement over the Tibetan Plateau.

10 **Keywords:** ATAL, condensational growth, COBALD

11

12 **1. Introduction**

13 The Asian Tropopause Aerosol Layer (ATAL) extends over a large area within the
14 Asian summer monsoon circulation and may significantly influence ozone, cirrus
15 clouds and global climate by chemical, micro-physical and radiative processes
16 [Gettelman et al., 2011; Vernier et al., 2011; Fadnavis et al., 2013; Thomason and
17 Vernier, 2013; Vernier et al., 2015]. Particles in the ATAL are likely to be lifted to the
18 lower stratosphere by the large-scale upward circulation within the south Asian
19 anticyclone, and then influence the aerosol amount in the global stratosphere
20 significantly [Park et al., 2007]. Solomon et al. [2011] found that the radiative forcing
21 of increased aerosols in the global stratosphere from 2000 to 2010 is $-0.1\text{W}\cdot\text{m}^{-2}$, which
22 weakened the global warm effect from greenhouse gases.

23 In addition to the maximum concentration of aerosols found in the ATAL as
24 mentioned above, the concentrations of tropospheric trace gases (i.e., water vapor, CO,
25 CH₄ and HCN) are higher within the Asian summer monsoon anticyclone than in
26 surrounding regions, while the stratospheric trace gases (i.e, O₃, HNO₃ and HCl) are
27 lower [Park et al., 2004; Randel et al., 2010]. Actually, the maximum aerosol
28 concentration near the tropopause over the Tibetan Plateau has also been observed by
29 lidar and balloon borne measurements [Kim et al., 2003; Tobo et al., 2007; He et al.,



1 2014]. Li [2005] showed that the aerosol plume is detectable in the anticyclone around
2 the altitude of 150 hPa over the Tibetan Plateau through satellite observations and
3 model study.

4 The formation mechanism of ATAL has not been fully understood mainly due to
5 sparse in situ measurements. [Frey et al., 2011] proposed that nucleation events at very
6 low temperatures accompanied by the outflow of convective systems could be dominant
7 process in the production of ATAL. Vernier et al. [2015] found that there is a one-
8 month phase lag of the aerosol scattering ratio from the Cloud-Aerosol Lidar and
9 Infrared Pathfinder Satellite Observation (CALIPSO) after the relative humidity with
10 respect to ice (RHi) from the Microwave Limb Sounding (MLS) at the beginning of the
11 convective period (May/June), possibly due to the growth of the nanometric particles
12 to the larger particles that can be detected by satellites.

13 Both condensation and coagulation contribute to the particle growth, even though
14 these two processes are triggered by different mechanism. Model studies have shown
15 that the coagulation is more important than the nucleation in the control of the number
16 concentration of fine particles (with diameter larger than 10 nm) in the UTLS [English
17 et al., 2011; Pierce and Adams, 2009; Timmreck et al., 2010]. Except for coagulation,
18 the effect of condensation on particle growth is less documented in previous studies.
19 Weigel et al. [2011] found that supersaturated gases, which can nucleate to form neutral
20 and charged molecular clusters, also condense onto pre-existing aerosol particles and
21 cloud droplets. Earlier studies demonstrated that the stratospheric aqueous H_2SO_4
22 aerosol can absorb a large amount of gaseous HNO_3 and H_2O at temperatures (about
23 200K) between the nitric acid trihydrate (NAT) and ice frost points [Carslaw et al.,
24 1994; Tabazadeh et al., 1994], leading to a steep increase in particle volume.
25 Heterogeneous reactions are active on the extreme cold stratospheric aerosols and polar
26 stratospheric clouds (PSCs) over the winter poles. These aerosols and PSCs are
27 composed either of supercooled ternary solution (STS) droplets ($\text{HNO}_3\cdot\text{H}_2\text{O}\cdot\text{H}_2\text{SO}_4$),
28 ice particles or solid hydrates (most likely NAT) and can grow to larger particles that
29 are easy to sediment [Voigt et al., 2008; Engel, 2013]. However, unlike the studies
30 about PSCs, the growth mechanism of the particles in the ATAL is still poorly described



1 due to the lack of sufficient observations.

2 In-depth investigations on the aerosol size distribution, chemical composition and
3 growth process are needed for a better understanding of the characteristics and
4 formation mechanism of ATAL. It is difficult to obtain much more information merely
5 by means of remote sensing measurements, such as satellite and lidar, because those
6 sensors are not sensitive to ultra-fine particles. In such case, balloon and/or air borne *in*
7 *situ* measurement provide an additional and even better tool for exploring the ATAL.
8 Using a balloon-borne optical particle counter at Lhasa, China, Tobo et al. (2007)
9 measured the vertical profiles of aerosols and found occurrences of relatively high
10 number concentrations of sub-micron size aerosols near the tropopause region during
11 the Asian summer monsoon period. They considered that the enhanced aerosol layer in
12 the UTLS connected closely with the transportation of water vapor from the Asian
13 summer monsoon. An increased amount of water vapor was found in the UTLS within
14 the Asian summer monsoon anticyclone (Bian et al., 2012; Li et al., 2017). Recently, a
15 climate model simulation demonstrated that the abundant anthropogenic aerosol
16 precursor emissions from Asia coupled with rapid vertical transport associated with
17 monsoon convection could lead to significant particle formation in the upper
18 troposphere within the ASM anticyclone (Yu et al., 2017). More Recently, a series of
19 balloon borne activities over India and Saudi Arabia during the Balloon Measurements
20 of the Asian Tropopause Aerosol Layer (BATAL) campaigns revealed that the ATAL
21 is composed of mostly small ($r < 0.25 \mu\text{m}$) liquid (~80%–95%) aerosols with the
22 dominant composition of nitrate (Vernier et al., 2017).

23 As part of the project Tibetan Ozone, Aerosol and Radiation (TOAR) [see More
24 Information on ACP Special Issue, available at: [http://www.atmos-chem-](http://www.atmos-chem-phys.net/special_issue331.html)
25 [phys.net/special_issue331.html](http://www.atmos-chem-phys.net/special_issue331.html)], the vertical profiles of aerosols over the southeastern
26 Tibetan Plateau were measured in June and July of 2014. In this paper, we present the
27 results from balloon borne radiosonde measurements, and investigate the contribution
28 of condensational growth by gas-to-particle conversion processes to the observed high
29 concentrations of fine particles in the UTLS over the Tibetan Plateau.

30



1 2. Experiment

2 The field experiment was carried out at the Linzhi Meteorological Bureau (29.67°
3 N, 94.33° E; 2992 m MSL), located in the southeastern Tibetan Plateau, from June 6 to
4 July 31, 2014. During the field campaign, seven balloon sondes were launched, with
5 each sounding taking place at about 16:00 UTC on June 18 (case 1), June 24 (case 2),
6 July 6 (case 3), July 15 (case 4), July 21 (case 5), July 25 (case 6) and July 30 (case 7),
7 respectively. The balloon sonde payload was composed of the Compact Optical
8 Backscatter Aerosol Detector (COBALD) particle backscatter sonde, the IMet and
9 RS92 radiosonde, and the cryogenic frost-point hygrometer (CFH). The payload was
10 lifted by a 1600 g latex balloon, which flew at an ascent rate of 5-7 m s⁻¹. Data were
11 obtained from the launching point until an altitude between 30 km to 35 km where the
12 balloon generally burst. In this study, only the ascending data are analyzed.

13 2.1 COBALD particle backscatter sonde

14 The lightweight COBALD, developed by Prof. Thomas Peter's group at ETH
15 Zurich, uses two high power light emitting diodes (LEDs) operating at 455nm (blue)
16 and 940nm (infrared) with a silicon detector averaging the light scattered back from
17 molecules or aerosols at angles centered near 173° for typically one second time
18 periods [Rosen and Kjome, 1991; Wienhold, 2012; Cirisan et al., 2014]. COBALD
19 measurements are only carried out at local nighttime as daylight saturates the sensitive
20 detector.

21 Backscatter ratios (BSR) at two wavelengths are retrieved from COBALD
22 measurement, which is defined as follow,

$$23 \quad BSR = \frac{\beta_a + \beta_m}{\beta_m} = \frac{N_a \cdot \sigma_a + N_m \cdot \sigma_m}{N_m \cdot \sigma_m} \quad (1)$$

24 where β denotes backscatter coefficient, N the number concentration, and σ the
25 backscatter cross section. The subscripts a and m indicate contributions from aerosol
26 particles and air molecules, respectively. The backscatter cross section for air molecules
27 can be calculated from Rayleigh scatter theory and the number concentration for air
28 molecules is derived from atmospheric pressure and temperature measured by the
29 radiosonde. From the COBALD raw data the blue and infrared backscatter ratio of each



1 individual flight profile was derived with an accuracy of 5 % and the precision in an
2 order of 1% [Vernier et al., 2015]. The backscattering cross section for aerosol particles
3 can be calculated from Mie scatter theory for a specified effective radius. The aerosol
4 backscatter ratio (ABSR) is defined as,

$$5 \quad ABSR = \frac{\beta_a}{\beta_m} = BSR - 1 \quad (2)$$

6 The ABSR values at two wavelengths are used to calculate the Color Index [CI,
7 Rosen et al., 1997], which is defined as the ABSR at 940 nm divided by the ABSR at
8 455 nm. The CI is proportional to the ratio of the backscatter cross sections at 940 and
9 455 nm, and hence it can provide an estimate of the particle size. Assuming an index
10 of refraction of 1.45 with 75% sulfate and a typical lognormal size distribution of the
11 stratospheric aerosols [Rosen and Kjöme, 1991], the backscatter cross sections σ_a at the
12 wavelengths used by COBALD are calculated by Mie theory, and further the CI as a
13 function of the mean radius of total aerosol particles is derived. Because no information
14 on standard deviation of the lognormal distribution is available, the possible lower and
15 upper limits the standard deviation are assumed to be 1.8 and 2.2 [Deshler et al., 2003].
16 By comparing the observed CI with the calculated one for different standard deviations,
17 the range of possible mean radius can be obtained, and the number concentration and
18 further volume concentration for aerosol particles can be retrieved from the observed
19 ABSR according to the Equation (1).

20 **2.2 Radiosonde observations**

21 In this study we use the air temperature profiles from the RS92 radiosondes with
22 an uncertainty of $\pm 0.2^\circ\text{C}$ below 100 hPa and $\pm 0.3^\circ\text{C}$ between 100 and 20 hPa. The
23 profiles of water vapor are obtained from CFH measurements. The CFH is a
24 microprocessor-controlled instrument with a lightweight of 400 g, and it uses a
25 cryogenic liquid as cooling agent and operates based on the chilled-mirror principle
26 [Vömel et al., 2007a]. The uncertainty of frost point or dew point measured by the CFH
27 is smaller than 0.2 K. Correspondingly, the uncertainty in relative humidity is estimated
28 to be 2 % for measurement in the lower troposphere and 5 % in the tropical tropopause
29 region [Vömel et al., 2016]. As a standard for water vapor measurements, CFH has

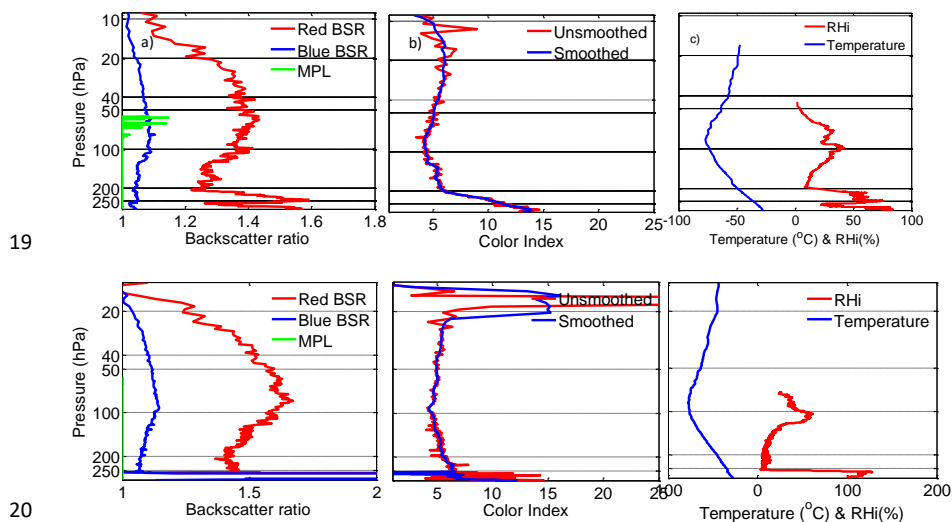


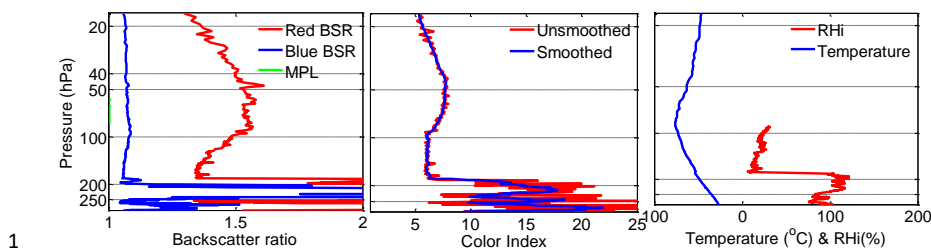
1 been used in numerous intercomparison experiments, such as the validation of Aura
2 Microwave Limb Sounder (MLS) water vapor products, globally [Vömel et al., 2007b]
3 and specifically over the Tibetan Plateau [Yan et al., 2016].

4

5 **3. Results and discussion**

6 Figure 1 shows the BSR profiles at two wavelengths and calculated CI profiles
7 from COBALD measurement, as well as the profiles of temperature and RH over ice
8 respectively from RS92 and CFH measurement for three typical cases on June 18, July
9 15 and 25, 2014. The COBALD measurements suggest an enhanced aerosol layer (BSR
10 (455 nm) >1.1 and BSR (940 nm) >1.4) extending from 200 hPa (~12 km) to 10hPa (~28
11 km) with a maximum above the tropopause (90 hPa, ~17 km). The RHi near the
12 maximum of the enhanced aerosol layer varies from 30% to 40%, indicating that it is
13 impossibly caused by cirrus cloud, which cannot persist at these dry conditions. It
14 should be noted that the volcanic eruption might have negligible influence on the
15 observed aerosol layers as no volcanic eruption occurred during the experiment period.
16 The calculated CI of the enhanced aerosol layer is around 5 (4 - 8), far below CI of
17 cirrus cloud (being around 10 with the maximum value exceeding 20) at 250 hPa
18 [Vernier et al., 2015].

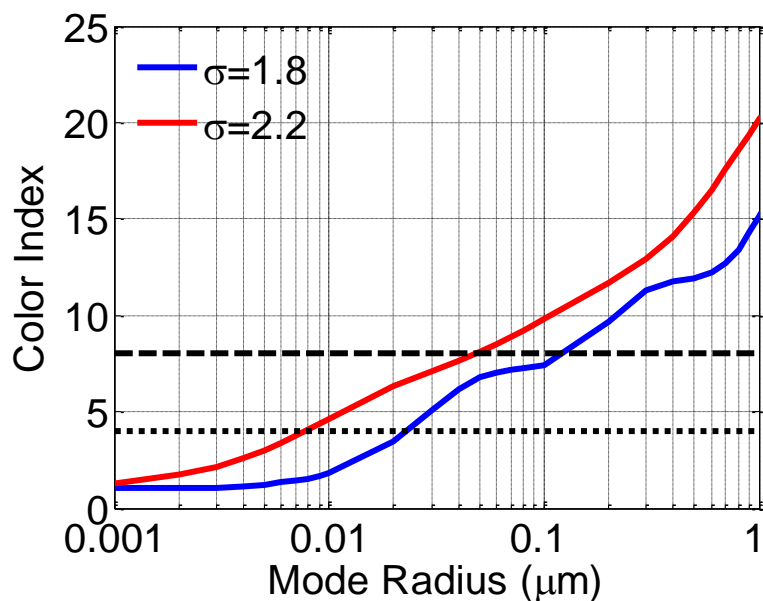




1
2 **Fig. 1.** (a) Three cases of the backscattering ratio profile from COBALD and MPL
3 measurements on June 18 (top), July 15 (middle) and July 25 (bottom), 2014. (b) The
4 calculated CI profiles from the ABSR at two wavelengths. (c) Temperature and RH
5 profiles measured by the RS92 radiosonde and CFH, respectively.

6

7 Pinnick et al. [1975] adopted a lognormal distribution with a mode radius of 0.0725
8 μm and standard deviation (σ) of 1.86 to parameterize the background aerosols in the
9 stratosphere. Rosen and Kjome [1991] suggested a mode radius between 0.04 and 0.06
10 μm and σ value of ~ 2.0 -2.2 for the 20-km stratospheric aerosol background layer. In
11 this study, the CI as a function of mode radius was derived from Mie calculation using
12 a lognormal distribution for different size of aerosols with standard deviations (σ) of
13 1.8 and 2.2 respectively and the result is shown in Fig. 2. The CI increases
14 monotonously from 1 to 15 with mode radius growing from 1 nm to 1 μm . The CI of
15 the enhanced aerosol layer from COBALD measurement usually varied from 4 to 8 as
16 indicated in this figure. With the assumed lognormal widths, the measured CI imposes
17 an upper limit of 100 nm on the particle radius. Therefore, we conclude that the
18 enhanced aerosol layer is composed of a large number of fine particles with radius less
19 than 0.1 μm . It has been documented that aerosols in the UTLS are mainly composed
20 of liquid inorganics with typical mode radii smaller than 0.1 μm [Tobo et al., 2007].
21 Our observations in Linzhi are consistent with previous findings.



1
2 **Fig. 2.** CI as a function of mode radius from Mie calculation assuming an index of
3 refraction of 1.45 and a lognormal size distribution with the indicated standard
4 deviations (σ) of 1.8 and 2.2. The dotted and dashed lines represent the minimum (~ 4)
5 and maximum (~ 8) CI of the enhanced aerosol layer from COBALD measurement for
6 all cases.

7
8 The middle troposphere over the Tibetan Plateau is likely to act as a pipe for the
9 transport of water vapor from the marine boundary layer (i.e., Indian Ocean and South
10 China Sea) to the UTLS, leading to an increase of H₂O mixing ratio near the tropopause
11 [Fu et al., 2006; Lelieveld et al., 2007]. Figure 3(a) presents the CFH H₂O profiles from
12 110 hPa (~ 16 km ASL) to 90 hPa (~ 17.5 km ASL). It is noticed that H₂O concentration
13 changes greatly in the vertical direction (3–12 ppmv) for some cases. The dehydration
14 process results in minimum H₂O concentration just above the altitude of each lowest
15 temperature. Pronounced decrease of the H₂O concentration from 110 hPa to 90 hPa
16 are attributed to convection transport of moist air parcels just occurring during the
17 balloon flying periods. The three relatively uniform H₂O profiles (on June 18, July 25
18 & 30) correspond to the well mixed status of strong upward transport prior to the
19 balloon-based measurements. The water vapor cycle driven by synoptic-scale



1 convection increases the possibility of the condensational growth of aerosols near the
2 tropopause over the Tibetan plateau. It has been estimated that the scattering ratio could
3 increase by 10% to 50% with a water vapor mixing ratio enhancement from 3 ppmv to
4 6 ppmv [Vernier et al., 2011].

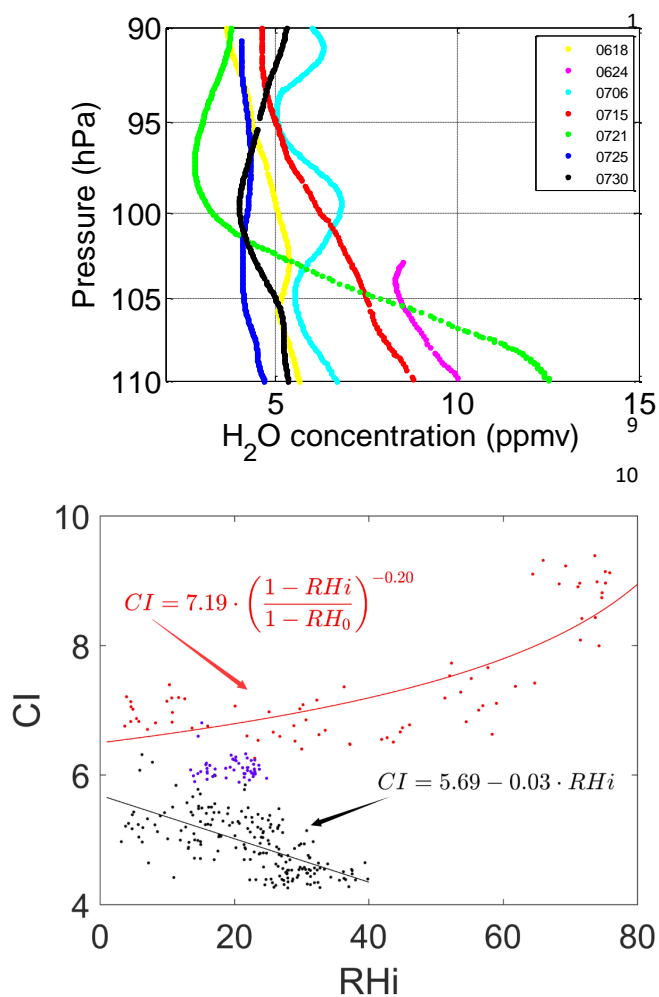
5 Fig. 3(b) presents the variation of CI with RH_i for all cases between 50 hPa and
6 150 hPa, the typical altitude range for the ATAL. The dependency of CI on RH_i can be
7 classified into three types according to the CI of dry aerosols, i.e. the aerosols existing
8 at very low relative humidity (e.g., RH_i < 20%):

9 (1) When the CI of dry aerosol is larger than about 6, CI of the enhanced aerosol
10 layer shows an exponential growth with increasing RH_i;

11 (2) When the CI of dry aerosol is smaller than about 6, CI of the enhanced aerosol
12 layer decreases with increasing RH_i in a slope of -0.03;

13 (3) When the CI of dry aerosol is close to 6, it keeps almost constant with variation
14 of RH_i.

15 As the CI can be regarded as an indicator of aerosol particle size, it can be inferred
16 that for those aerosol particles with large dry sizes (Type 1, i.e., CI > 6), increasing RH_i
17 facilitates water vapor and other gaseous precursors to condense onto pre-existing
18 aerosol particles and then contribute to the particle growth. For those with small dry
19 sizes (Type 2 and Type 3, i.e., CI ≤ 6), the situation appears to be more completed and
20 cannot be fully understood without more detailed information about aerosol chemical
21 composition and their gas precursors. Since all these aerosol particles were observed at
22 very low RH_i, well below 40% deliquescence relative humidity of most of the salts
23 (e.g., 40% for NH₄HSO₄) [Benson et al., 2009], the condensation of water vapor should
24 have negligible effect on the growth of these particles. New particle formation through
25 the gas-to-particle conversion process, which tends to become faster with increasing
26 RH [Fountoukis and Nenes, 2007], increases the number concentration, resulting in
27 decrease of mode radius of bulk aerosols. Therefore, the decrease of CI with RH_i (Type
28 2) indicates that new particle formation might play an important role in the formation
29 and prevalence of fine particles in the UTLS over the Tibetan Plateau.

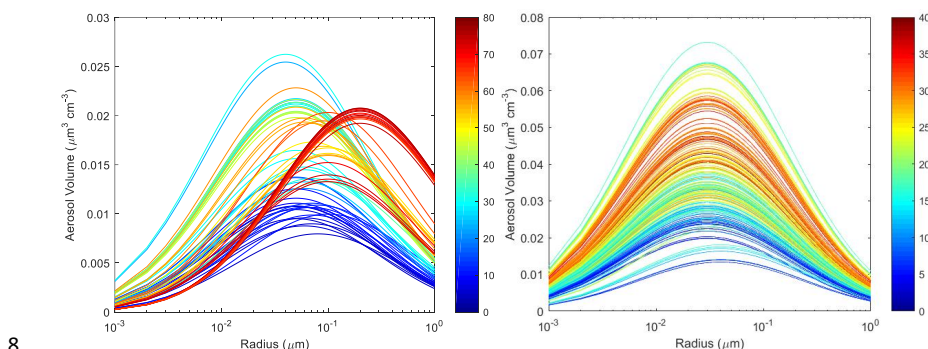


11
 12 **Fig. 3.** (a) H₂O concentration from CFH measurements, and (b) the variation of CI with
 13 RH_i between 50 hPa and 150 hPa for all cases. The two fitted equations all exceeding
 14 the 99% significance level.

15
 16 Based on the BSR and CI at the UTLS altitudes (50-150 hPa) from COBALD, we
 17 calculated the aerosol volume concentration in the enhanced aerosol layer for the two
 18 typical CI variation trend according to an assumption of lognormal size distribution
 19 with standard deviation of 1.8. The variation of aerosol volume concentration
 20 distributions with RH_i is shown in Fig. 4. It can be seen from Fig 4a that when RH_i is
 21 less than 60%, aerosol mode radius ranges mostly between 0.04 and 0.07 μm, and it



1 increases steeply to $0.2 \mu\text{m}$ when RHi is more than 60%. The aerosol volume
2 concentrations are obviously high compared with those in dry condition, especially for
3 those particles with a mode radius of $0.1 \mu\text{m}$. For those aerosols with small initial dry
4 particle size (as shown in Fig 4b), accompanied by a mode radius decrease from 0.04
5 to $0.03 \mu\text{m}$, the aerosol volume concentration increases by 4-5 times when RHi rises
6 from nearly zero to 40%, indicating that the number concentrations experience an
7 explosive growth due to the formation of new particles.



8
9 **Fig. 4.** The variation of aerosol volume concentration distributions in the enhanced
10 aerosol layer with RHi for (a) case 5 (July 21), and (b) the other cases corresponding to
11 the black dots in Fig 3b. The color of each distribution represents RHi labeled on the
12 color bar.

13

14 4. Conclusions

15 The vertical profiles of aerosol BSR measured over the Tibetan Plateau during
16 summertime demonstrate an enhanced aerosol layer, consisting predominantly of fine
17 particles with mode radius smaller than $0.1 \mu\text{m}$, in the UTLS. The size of particles in
18 the enhanced aerosol layer shows an exponential increase with increasing RHi when
19 the CI of dry aerosols is larger than 6 (corresponding mode radius larger than $0.04 \mu\text{m}$).
20 It can be inferred that for increasing RHi leads to the condensation of water vapor and
21 other gaseous precursor onto pre-existing aerosol particles and contributes to the
22 particle growth. For the CI of dry aerosols smaller than about 6 (i.e., mode radius
23 smaller than $0.04 \mu\text{m}$), the size of particles in the enhanced aerosol layer decreases with



1 increasing RHi. In this case, more new particle formation, which results in a decrease
2 of aerosol mode radius and increase of number concentration, can play an important
3 role in the accumulation of large amounts of fine particles in the UTLS over the Tibetan
4 Plateau. Chemical interactions involved in the stratosphere troposphere exchange are
5 complicated and further experimental and model studies are needed to understand the
6 nature and origin of ATAL and its influence on global atmospheric chemistry and
7 climate.

8

9 **Author Contributions**

10 Qianshan He, Jianzhong Ma and Xiangdong Zheng designed the study. Holger Vömel
11 and Frank G. Wienhold respectively contributed to data quality control of COBALD
12 and CFH. Guangming Shi calculated Mie scattering parameters. Wei Gao, Dongwei
13 Liu and Tiantao Cheng contributed to data analysis, numerical experiments,
14 interpretation and paper writing. Qianshan He did further analysis and interpreted the
15 results. All authors contributed to improve the manuscript.

16

17 *Acknowledgements.* This study was supported by the National Natural Science
18 Foundation of China (Grant No. 91637101) and the Shanghai Science and Technology
19 Committee Research Project (Grant No. 16ZR1431700). We thank all TOAR team
20 members and the staff from the Tibet Meteorological Service for assisting our
21 experiment work. We also thank Dr. Yutaka Tobo, whose useful suggestions have
22 greatly improved the paper.

23

24

25 **References**

- 26 Benson, D. R., Erupe, M. E., and Lee, S. H.: Laboratory-measured $\text{H}_2\text{SO}_4\text{-H}_2\text{O-NH}_3$
27 ternary homogeneous nucleation rates: Initial observations, *Geophys. Res. Lett.*,
28 36, 10.1029/2009gl038728, 2009.
- 29 Bian, J., Pan, L. L., Paulik, L., Vmel, H., Chen, H., and Lu, D.: In situ water vapor
30 and ozone measurements in Lhasa and Kunming during the Asian summer



- 1 monsoon, *Geophys. Res. Lett.*, 39(19), 19808, 2012.
- 2 Carslaw, K. S., Luo, B. P., Clegg, S. L., Peter, T. H., Brimblecombe, P., and Crutzen, P.
3 J.: Stratospheric aerosol growth and HNO₃ gas phase depletion from coupled
4 HNO₃ and water uptake by liquid particles, *Geophys. Res. Lett.*, 21, 2479 – 2482,
5 1994.
- 6 Cirisan, A., Luo, B. P., Engel, I., Wienhold, F. G., Krieger, U. K., Weers, U., Romanens,
7 G., Levrat, G., Jeannet, P., Ruffieux, D., Philipona, R., Calpini, B., Spichtinger,
8 P., and Peter, T.: Balloon-borne match measurements of mid-latitude cirrus clouds,
9 *Atmos. Chem. Phys.*, 14, 7341–7365, 2014.
- 10 Deshler, T., Hervig, M. E., Hofmann, D. J., Rosen, J. M., and Liley, J. B.: Thirty years
11 of in situ stratospheric aerosol size distribution measurements from Laramie,
12 Wyoming (41N), using balloon-borne instruments, *J. Geophys. Res.*, 108,
13 doi:10.1029/2002JD002514, 2003.
- 14 Engel, I.: The Role of Heterogeneous Nucleation in Polar Stratospheric Cloud
15 Formation: Microphysical Modeling, ETH ZURICH, Doctor Dissertation, 2013.
- 16 English J. M., Toon, O. B., Mills, M. J., and Yu, F.: Microphysical simulations of new
17 particle formation in the upper troposphere and lower stratosphere, *Atmos. Chem.*
18 *Phys.*, 11, 9303–9322, 2011.
- 19 Fadnavis, S., Semeniuk, K., Pozzoli, L., Schultz, M. G., Ghude, S. D., Das, S., and
20 Kakatkar, R.: Transport of aerosols into the UTLS and their impact on the Asian
21 monsoon region as seen in a global model simulation, *Atmos. Chem. Phys.*,
22 13(17), 8771-8786, 2013.
- 23 Fountoukis, C., and Nenes, A.: ISORROPIA II: a computationally efficient
24 thermodynamic equilibrium model for K⁺ -Ca²⁺ -Mg²⁺ -NH₄⁺ -Na⁺ -SO₄²⁻ -NO₃⁻
25 -Cl⁻ -H₂O aerosols, *Atmos. Chem. Phys.*, 7, 4639-4659, 10.5194/acp-7-4639-
26 2007, 2007.
- 27 Frey, W., Borrmann, S., Kunkel, D., and Cairo, F.: In-situ measurements of tropical
28 cloud properties in the West African monsoon: Upper tropospheric ice clouds,
29 mesoscale convective system outflow, and subvisual cirrus, *Atmos. Chem. Phys.*,
30 11, 5569–5590, doi:10.5194/acp-11-5569-2011, 2011.



- 1 Fu, R., Hu, Y., Wright, J. S., Jiang, J. H., Dickinson, R. E., Chen, M., Filipiak, M., Read,
2 W. G., Waters, J. W., and Wu, D. L.: Short circuit of water vapor and polluted air
3 to the global stratosphere by convective transport over the Tibetan Plateau, Proc.
4 Natl. Acad. Sci. U. S. A., 103, 5664–5669, doi:10.1073/pnas.0601584103, 2006.
- 5 Gettelman, A., Hoor, P., Pan, L. L., Randel, W. J., Hegglin, M. I., and Birner, T.: The
6 extratropical upper troposphere and lower stratosphere, Rev. Geophys., 49(3),
7 RG3003, 2011.
- 8 He, Q. S., Li, C. C., Ma, J. Z., Wang, H. Q., Yan, X. L., Lu, J., Liang, Z. R., and Qi, G.
9 M.: Lidar-observed enhancement of aerosols in the upper troposphere and lower
10 stratosphere over the Tibetan Plateau induced by the Nabro volcano eruption,
11 Atmos. Chem. Phys., 14, 1-9, 2014.
- 12 Kim, Y. S., Shibata, T., Iwasaka, Y., Shi, G. Y., Zhou, X. J., Tamura, K., and Ohashi, T.:
13 Enhancements of aerosols near the cold tropopause in summer over Tibetan
14 Plateau: Lidar and balloon borne measurements in 1999 at Lhasa, Tibet, China.
15 Proc SPIE, 4893, 496-503, doi:10.1117/12.466090, 2003.
- 16 Lelieveld, J., Brühl, C., Jackel, P., Steil, B., Crutzen, P. J., Fischer, H., Giorgetta, M. A.,
17 Hoor, P., Lawrence, M. G., Sausen, R., and Tost, H.: Stratospheric dryness: model
18 simulations and satellite observations, Atmos. Chem. Phys., 7, 1313-1332,
19 doi:10.5194/acp-7-1313-2007, 2007.
- 20 Li, Q.: Trapping of Asian pollution by the Tibetan anticyclone: A global CTM
21 simulation compared with EOS MLS observations, Geophys. Res. Lett., 32,
22 L14826, doi:10.1029/2005GL022762, 2005.
- 23 Martinsson, B. G., Friberg, J., Andersson, S. M., Weigelt, A., Hermann, M., Assmann,
24 D., Voigtländer, B. C. A. M., van Velthoven, P. J. F., and Zahn, A.: Comparison
25 between CARIBIC aerosol samples analyzed by accelerator-based methods and
26 optical particle counter measurements, Atmos. Meas. Tech., 7, 2581–2596,
27 doi:10.5194/amt-7-2581-2014, 2014.
- 28 Li, D., Vogel, B., Bian, J., Müller, R., Pan, L. L., Günther, G., Bai, Z., Li, Q., Zhang,
29 J., Fan, Q., and Vömel, H.: Impact of typhoons on the composition of the upper
30 troposphere within the Asian summer monsoon anticyclone: the SWOP



- 1 campaign in Lhasa 2013, Atmos. Chem. Phys., 17, 4657-4672, 10.5194/acp-17-
2 4657-2017, 2017.
- 3 Park, M., Randel, W. J., Kinnison, D. E., Garcia, R. R., and Choi, W.: Seasonal variation
4 of methane, water vapor, and nitrogen oxides near the tropopause: Satellite
5 observations and model simulations, J. Geophys. Res., 109, D03302,
6 doi:10.1029/2003JD003706, 2004.
- 7 Park, M., Randel, W. J., Gettelman, A., Massie, S. T., and Jiang, J. H.: Transport above
8 the Asian summer monsoon anticyclone inferred from Aura Microwave Limb
9 Sounder tracers, J. Geophys. Res., 112, D16309, doi:10.1029/2006jd008294,
10 2007.
- 11 Pierce, J. R., and Adams, P. J.: Can cosmic rays affect cloud condensation nuclei by
12 altering new particle formation rates? Geophys. Res. Lett., 36, L09820,
13 doi:10.1029/2009GL037946, 2009.
- 14 Pinnick, R. G., Rosen, J. M., and Hofmann, D. J.: Stratospheric Aerosol Measurements
15 III: Optical Model Calculations, J. Atmos. Sci., 33, 304-314, 1975.
- 16 Randel, W. J., Park, M., Emmons, L., and Pumphrey, H. C.: Asian monsoon transport
17 of pollution to the stratosphere, Science, 328, 611-613,
18 doi:10.1126/science.1182274, 2010.
- 19 Rosen, J., and Kjome, N.: Backscattersonde: a new instrument for atmospheric aerosol
20 research, Appl. Opt., 30, 1552-1561, 1991.
- 21 Rosen, J., Kjome, N., and Liley, J.: Tropospheric aerosol backscatter at a midlatitude
22 site in the northern and southern hemispheres, J. Geophys. Res., 102, D17, 21329-
23 21339, 1997.
- 24 Solomon, S., Daniel, J. S., Neely III, R. R., Vernier, J. P., Dutton, E. G., and Thomason,
25 L. W.: The persistently variable background stratospheric aerosol layer and global
26 climate change, Science, 333, 866-870, doi:10.1126/science.1206027, 2011.
- 27 Schlager, H., and Arnold, F.: Measurement of stratospheric gaseous nitric acid in the
28 Winter arctic vortex using a novel rocket-borne mass spectrometer method,
29 Geophys. Res. Lett., 17, 433-436, 1990.
- 30 Tabazadeh, A., Turco, R. P., and Jacobson, M. Z.: A model for studying the composition



- 1 and chemical effects of stratospheric aerosols, *J. Geophys. Res.*, 99, 12897-12914,
2 1994.
- 3 Thomason, L. W., and Vernier, J. P.: Improved SAGE II cloud/aerosol categorization
4 and observations of the Asian tropopause aerosol layer: 1989-2005, *Atmos. Chem.*
5 *Phys.*, 13, 4605-4616, doi:10.5194/acp-13-4605-2013, 2013.
- 6 Timmreck, C., Graf, H. F., Lorenz, S. J., Niemeier, U., Zanchettin, D., Matei, D.,
7 Jungclaus, J. H., and Crowley, T. J.: Aerosol size confines climate response to
8 volcanic super-eruptions, *Geophys. Res. Lett.*, 37, L24705,
9 doi:10.1029/2010GL045464, 2010.
- 10 Tobo, Y., Iwasaka, Y., Shi, G. Y., Kim, S., Ohashi, T., Tamura, K., and Zhang, D. Z.:
11 Balloon-borne observations of high aerosol concentrations near the summertime
12 tropopause over the Tibetan Plateau, *Atmos. Res.*, 84, 233-241, doi:
13 10.1016/j.atmosres.2006.08.003, 2007.
- 14 Vernier, J. P., Thomason, L. W., and Kar, J.: CALIPSO detection of an Asian tropopause
15 aerosol layer, *Geophys. Res. Lett.*, 38, L07804, doi:10.1029/2010GL046614,
16 2011.
- 17 Vernier, J. P., Fairlie, T. D., Natarajan, M., Wienhold, F. G., Bian, J., Martinsson, B.
18 G., Crumeyrolle, S., Thomason, L. W., and Bedka, K. M.: Increase in upper
19 tropospheric and lower stratospheric aerosol levels and its potential connection
20 with Asian pollution, *J. Geophys. Res. Atmos.*, 120, 1608–1619,
21 doi:10.1002/2014JD022372, 2015.
- 22 Vernier, J. P., Fairlie, T. D., Deshler, T., Kumar, B. S., Natarajan, M., Pandit, A. K.,
23 Akhil Raj, S. T., Hemanth Kumar, A., Jayaraman, A., Singh, A., Rastogi, N.,
24 Sinha, P. R., Kumar, S., Tiwari, S., Wegner, T., Baker, N., Vignelles, D.,
25 Stenchikov, G., Shevchenko, I., Smith, J., Bedka, K., Kesarkar, A., Singh, V.,
26 Bhate, J., Ravikiran, V., Durga Rao, M., Ravindrababu, S., Patel, A., Vernier, H.,
27 Wienhold, F. G., Liu, H., Knepp, T. N., Thomason, L., Crawford, J., Ziemba, L.,
28 Moore, J., Crumeyrolle, S., Williamson, M., Berthet, G., Jégou, F., and Renard,
29 J. B.: BATAL: The Balloon measurement campaigns of the Asian Tropopause
30 Aerosol Layer. *Bulletin of the American Meteorological Society*, BAMS-D-17-



- 1 upper troposphere and lower–middle stratosphere over the Tibetan Plateau during
2 boreal summer, *Atmos. Meas. Tech.*, 9, 3547-3566, doi:10.5194/amt-9-3547-
3 2016, 2016.
- 4 Yu P., Rosenlof, K. H., Liu, S., Telg, H., and Gao, R. S.: Efficient transport of
5 tropospheric aerosol into the stratosphere via the Asian summer monsoon
6 anticyclone. *Proc. Nation. Acad. Sci.*, 114(27): 6972-6977, 2017.